Time-dependent Hartree-Fock calculations for grazing reactions at intermediate energy

Kazuyuki Sekizawa,[1,*] Jeffrey A. Tostevin,[2,†] and Kazuhiro Yabana[1,3,‡]

[1] *Graduate School of Pure and Applied Sciences, University of Tsukuba, Tsukuba 305-8571, Japan*
[2] *Department of Physics, Faculty of Engineering and Physical Sciences, University of Surrey, Guildford GU2 7XH, U.K.*
[3] *Center for Computational Sciences, University of Tsukuba, Tsukuba 305-8577, Japan*

(Dated: September 30, 2013)

We investigate applicability of the time-dependent Hartree-Fock (TDHF) theory to reactions at relatively high incident energy ($\sim$100 MeV/A). To this end, we consider nucleon transfer processes in grazing reaction at intermediate energies in ^{24}O+^{16}O system. To calculate reaction probabilities for specific transfer channels, we use a particle number projection method which was recently proposed by C. Simenel [Phys. Rev. Lett. **105**, 192701 (2010)]. Applying the particle number projection method, we also calculate excitation energy of a produced fragment in each transfer channel. From the calculation, we find that we can calculate grazing reaction up to around 100 MeV/A without numerical instability. However, in the case of incident energy of 200 MeV/A, there appear substantial problems. Energy dependences of the transfer probabilities and the excitation energies of produced fragments will be presented.

I. INTRODUCTION

Time-dependent Hartree-Fock (TDHF) theory is a microscopic theory for nuclear dynamics and has been successful to describe giant resonances and heavy-ion reactions. The theory of TDHF was first proposed by P.A.M. Dirac in 1930 [1] and its applications to nuclear collision dynamics started in the 1970s [2]. Since then, continuous efforts have been devoted for improving the method and extending applications (for a recent review, see Ref. [3]).

The TDHF theory enables us to describe heavy-ion collisions microscopically from nucleons' degrees of freedom in a self-consistent manner. Since parameters included in the effective interaction utilized in the TDHF calculation are determined to reproduce nuclear properties in a wide mass region, there is no adjustable parameter specific to the reaction dynamics. Nowadays, three-dimensional calculations with full Skyrme functionals including time-odd components with promising predictive power are becoming feasible [4]. Thus, the TDHF theory may be considered to be useful as a means to search for the preferable condition (projectile, target, and incident energy) to produce objective unstable nuclei far from the stability line.

However, since a many-body wave function in the TDHF theory is assumed to be a single Slater-determinant at all times, correlation effects beyond the mean-field level, such as nucleon-nucleon collisions and pairing correlations, are not taken into account in its framework. As increasing the incident energy, the mean free path becomes shorter than a diameter of a nucleus and the effect of nucleon-nucleon collisions becomes important. May be due to this fact, applications of the TDHF theory have been limited to reactions at relatively low incident energies ($\lesssim$ 10 MeV/A).

Nevertheless we noticed the above mentioned drawback of the framework, in the project work, we investigate nuclear reactions at relatively high incident energies ($\sim$100 MeV/A) employing the TDHF theory. The main points at issue are the following: (*i*) Is there any numerical/computational difficulty to perform a TDHF calculation at such a relatively high incident energy of around 100 MeV/A? (*ii*) If not, is it possible to describe reasonably a grazing reaction at the intermediate energy in the framework of the TDHF theory? The main goal of this work is to clarify how the TDHF theory works for reactions at such an intermediate energy.

To this end, we performed TDHF calculations for grazing reactions at several incident energies in ^{24}O+^{16}O system. Because the projectile ^{24}O contains additional eight neutrons compared to the target ^{16}O, transfer of neutrons (protons) from ^{24}O to ^{16}O (vise versa) is expected to occur. To extract transfer probabilities from the TDHF wave function after the collision, we use a particle number projection method which was recently proposed by C. Simenel [5]. By applying the particle number projection method, we also calculate excitation energy of produced fragment in each transfer channel. Comparing results of the TDHF calculation at different incident energies, numerical accuracy of the calculation will be discussed.

The construction of this paper is as follows. In Section II, we describe the main formalisms to analyze the grazing reaction in the TDHF theory. In Section III, we present results of our TDHF calculations for grazing reactions of ^{24}O+^{16}O. In Section IV, a summary and a future prospect will be presented.

* sekizawa@nucl.ph.tsukuba.ac.jp
† j.tostevin@surrey.ac.uk
‡ yabana@nucl.ph.tsukuba.ac.jp

II. FORMULATION

A. Nucleon transfer processes in the TDHF theory

First, let us explain a situation which we consider now. We consider a collision of two nuclei described by the TDHF theory. The projectile is composed of $N_{\rm P}$ nucleons and the target is composed of $N_{\rm T}$ nucleons. The total number of nucleons is $N = N_{\rm P} + N_{\rm T}$. In the TDHF calculation, a time evolution of single-particle orbitals, $\phi_i(\boldsymbol{r},\sigma,t)$ $(i = 1,\cdots,N)$, is calculated where $\boldsymbol{r}$ and σ denote the spatial and the spin coordinates, respectively. The total wave function is expressed as the Slater-determinant composed of the orbitals:

$$\Phi(x_1,\cdots,x_N,t) = \frac{1}{\sqrt{N!}}\det\{\phi_i(x_j,t)\}, \tag{1}$$

where x denotes a set of the spatial and the spin coordinates, $x \equiv (\boldsymbol{r},\sigma)$. For simplicity, we first consider a many-body system composed of identical fermions neglecting the isospin degrees of freedom. In Sec. II D, we discuss a projection method for actual nuclei composed of two kinds of fermions (neutrons and protons) to analyze excitation energy of produced fragments after the collision.

Before the collision, two nuclei are separated spatially. We divide the whole space into two, the projectile region, $V_{\rm P}^i$, and the target region, $V_{\rm T}^i$. After the collision, we assume that there appear two nuclei, a projectile-like fragment (PLF) and a target-like fragment (TLF). We ignore channels in which nuclei are separated into more than two fragments after the collision. We again introduce a division of the whole space into two, the projectile region, $V_{\rm P}^f$, which includes the PLF, and the target region, $V_{\rm T}^f$, which includes the TLF.

We define the number operator of each spatial region as

$$\hat{N}_\tau = \int_\tau d\boldsymbol{r}\ \sum_{i=1}^{N}\delta(\boldsymbol{r}-\boldsymbol{r}_i) = \sum_{i=1}^{N}\Theta_\tau(\boldsymbol{r}_i), \tag{2}$$

where τ specifies the spatial region either $V_{\rm P}^{i(f)}$ or $V_{\rm T}^{i(f)}$. We introduce the space division function, $\Theta_\tau(\boldsymbol{r})$, defined as

$$\Theta_\tau(\boldsymbol{r}) = \begin{cases} 1 & \text{for } \boldsymbol{r}\in\tau \\ 0 & \text{for } \boldsymbol{r}\notin\tau \end{cases}. \tag{3}$$

The sum of the two operators, $\hat{N}_{V_{\rm P}^{i(f)}}$ and $\hat{N}_{V_{\rm T}^{i(f)}}$, is the number operator of the whole space, $\hat{N} = \hat{N}_{V_{\rm P}^i} + \hat{N}_{V_{\rm T}^i} = \hat{N}_{V_{\rm P}^f} + \hat{N}_{V_{\rm T}^f}$. In ordinary TDHF calculations, an initial wave function is the direct product of the ground state wave functions of two nuclei boosted with the relative velocity. The single-particle orbitals, $\phi_i(x,t)$, are localized in one of the spatial regions, $V_{\rm P}^i$ or $V_{\rm T}^i$, at the initial stage of the calculation. Therefore, the initial wave function is the eigenstate of both operators, $\hat{N}_{V_{\rm P}^i}$ and $\hat{N}_{V_{\rm T}^i}$, with eigenvalues, $N_{\rm P}$ and $N_{\rm T}$, respectively. At the final stage of the calculation after the collision, each single-particle orbital extends spatially to both spatial regions of $V_{\rm P}^f$ and $V_{\rm T}^f$. Due to this fact, the Slater determinant at the final stage is not an eigenstate of the number operators, $\hat{N}_{V_{\rm P}^f}$ and $\hat{N}_{V_{\rm T}^f}$, but a superposition of states with different particle number distributions. We can then calculate probabilities for certain particle number distributions at the final stage of calculation.

B. Number projection operator

In our paper [4], we used the particle number projection method which was recently proposed by C. Simenel [5]. In the method, the probability that n nucleons are in the spatial region $V_{\rm P}^f$ and $N-n$ nucleons are in the spatial region $V_{\rm T}^f$ can be calculated as follows. Let us denote a many-body wave function at the final stage of the calculation, at time $t = t_f$, as

$$\Psi(x_1,\cdots,x_N) = \frac{1}{\sqrt{N!}}\det\{\psi_i(x_j)\}, \tag{4}$$

and omit the time index, t_f. Here and hereafter, we also omit the suffix f from two spatial regions at the final stage of the calculation, $V_{\rm P}^f$ and $V_{\rm T}^f$. We use the particle number projection operator given by

$$\hat{P}_n = \frac{1}{2\pi}\int_0^{2\pi} d\theta\ e^{i(n-\hat{N}_{V_{\rm P}})\theta}. \tag{5}$$

This operator extracts a component of wave function in which an expectation value of the number operator in the spatial region $V_{\rm P}$ equals to n. By taking an expectation value of the particle number projection operator, Eq. (5), we can calculate the probability that n nucleons are in the spatial region $V_{\rm P}$ and $N-n$ nucleons are in the spatial region $V_{\rm T}$, as follows:

$$\begin{aligned} P_n &\equiv \langle\Psi|\,\hat{P}_n\,|\Psi\rangle \\ &= \frac{1}{2\pi}\int_0^{2\pi} d\theta\ e^{in\theta}\det\big\{\langle\psi_i|\psi_j\rangle_{V_{\rm T}} + e^{-i\theta}\langle\psi_i|\psi_j\rangle_{V_{\rm P}}\big\}, \end{aligned} \tag{6}$$

where $\langle\psi_i|\psi_j\rangle_\tau \equiv \sum_\sigma\int d\boldsymbol{r}\psi_i^*(\boldsymbol{r},\sigma)\psi_j(\boldsymbol{r},\sigma)$ denotes an overlap integral between two orbitals $\psi_i(x)$ and $\psi_j(x)$ in the spatial region $\tau = V_{\rm P}$ or $V_{\rm T}$. From the probability P_n, we may obtain nucleon transfer probabilities. For example, the probability of n-particle transfer from the projectile to the target is given by $P_{N_{\rm P}-n}$.

C. Expectation value in particle number projected states

We next discuss how to calculate expectation values of any operator by particle number projected states. In our

paper [4], we showed that the TDHF theory may describe the multinucleon transfer cross sections in a quality comparable to existing direct reaction theories. Then, one may be interested in not only inclusive quantities integrated over the impact parameter but also more exclusive quantities associated with each impact parameter in each transfer channel.

Let us consider an expectation value of an arbitrary operator, $\hat{\mathcal{O}}$, by a particle number projected state. We may calculate the expectation value of the operator $\hat{\mathcal{O}}$ by a particle number projected state in which n nucleons are included in the spatial region $V_{\rm P}$ after the collision by applying the particle number projection operator, as follows:

$$\begin{aligned}\mathcal{O}_n &\equiv \frac{\langle\Psi|\,\hat{\mathcal{O}}\hat{P}_n\,|\Psi\rangle}{\langle\Psi|\,\hat{P}_n\,|\Psi\rangle} \\ &= \frac{1}{2\pi P_n}\int_0^{2\pi} d\theta\; e^{in\theta}\,\langle\Psi|\,\hat{\mathcal{O}}e^{-i\hat{N}_{V_{\rm P}}\theta}\,|\Psi\rangle \\ &= \frac{1}{2\pi P_n}\int_0^{2\pi} d\theta\; e^{in\theta}\,\langle\Psi|\,\hat{\mathcal{O}}\,|\Psi(\theta)\rangle\,, \end{aligned} \tag{7}$$

where $\Psi(\theta)$ denotes a Slater determinant composed of single-particle wave functions whose component in the spacial region $V_{\rm P}$ is multiplied by a phase factor $e^{-i\theta}$. It can be expressed as

$$\Psi(x_1,\cdots,x_N,\theta) = \frac{1}{\sqrt{N!}}\det\{\psi_i(x_j,\theta)\} \tag{8}$$

$$\psi_i(x,\theta) = \Big(\Theta_{V_{\rm T}}(\boldsymbol{r}) + e^{-i\theta}\Theta_{V_{\rm P}}(\boldsymbol{r})\Big)\psi_i(x). \tag{9}$$

Because of the multiplication of the phase factor $e^{-i\theta}$, the single-particle orbitals, $\psi_i(x)$ and $\psi_i(x,\theta)$, are no longer orthonormal to each other, i.e. $\langle\psi_i|\psi_j(\theta)\rangle \neq \delta_{ij}$. We can calculate transitional matrix elements between two Slater-determinants composed of different kinds of orbitals which are non-orthonormal to each other [6]. Eq. (7) can be calculated as

$$\mathcal{O}_n = \frac{1}{2\pi P_n}\int_0^{2\pi} d\theta\; e^{in\theta}\det\mathcal{B}(\theta)\big\langle\Psi\big|\hat{\mathcal{O}}\big|\tilde{\Psi}(\theta)\big\rangle, \tag{10}$$

where $\mathcal{B}(\theta)$ denotes a N-dimensional matrix having matrix elements of $\langle\psi_i|\psi_j(\theta)\rangle$ on i-th row, j-th column. $\tilde{\Psi}(\theta)$ denotes a Slater-determinant composed of transformed single-particle wave functions which are orthonormal to ψ_i, i.e. $\big\langle\psi_i\big|\tilde{\psi}_j(\theta)\big\rangle = \delta_{ij}$, which is defined as

$$\tilde{\Psi}(x_1,\cdots,x_N,\theta) = \frac{1}{\sqrt{N!}}\det\{\tilde{\psi}_i(x_j,\theta)\} \tag{11}$$

$$\tilde{\psi}_i(x,\theta) = \sum_{k=1}^{N}\psi_k(x,\theta)\Big(\mathcal{B}(\theta)\Big)^{-1}_{ki}. \tag{12}$$

Since the two Slater determinants, Ψ and $\tilde{\Psi}(\theta)$, are composed of biorthonomal single-particle wave functions, we can calculate the transition matrix element between the two Slater-determinants, $\big\langle\Psi\big|\hat{\mathcal{O}}\big|\tilde{\Psi}(\theta)\big\rangle$, in a usual way. In principle, we can calculate an expectation value of any operators by particle number projected states by using Eqs. (10-12).

D. Excitation energy of each transfer channel

In this project work, the formulas described in the previous subsection, Eqs. (10-12), are applied to evaluate excitation energy of produced fragment after the collision. Here, we explain our approach to evaluate the excitation energy of produced fragment in each transfer channel [7]. It can be divided into the following three procedures: (*i*) Remove kinetic energy associated with a translational relative motion of center-of-masses of produced fragments. (*ii*) Calculate internal energy of the fragments applying the particle number projection method described in Sec. II C. (*iii*) Evaluate excitation energy by subtracting the ground state energy of a nucleus with the same neutron and proton numbers as the particle number projected state.

***Step* (*i*):** To calculate excitation energy of the produced fragment, we need to evaluate internal energy of each fragment with a certain number of nucleons. Because, in the TDHF theory, states in different transfer channels feel a single mean-field potential with a certain relative velocity, it is not at all obvious that how to remove kinetic energy of center-of-mass relative motion from total energy of each particle number projected state. To avoid this problem, we first "stop" the translational relative motion of the fragments by multiplying two plane waves $e^{-i\boldsymbol{K}_{\rm PLF}\cdot\boldsymbol{r}}$ to the wave function in the spatial region $V_{\rm P}$ and $e^{-i\boldsymbol{K}_{\rm TLF}\cdot\boldsymbol{r}}$ to the wave function in the spatial region $V_{\rm T}$. Denoting the mass and coordinate of the PLF at the final stage of the calculation as $M_{\rm PLF}$ and $\boldsymbol{R}_{\rm PLF}(t_f)$, respectively, the wave vector of the PLF is evaluated as $\boldsymbol{K}_{\rm PLF} = M_{\rm PLF}\dot{\boldsymbol{R}}_{\rm PLF}(t_f)/\hbar$, where $\dot{\boldsymbol{R}}_{\rm PLF}(t_f) \equiv \big(\boldsymbol{R}_{\rm PLF}(t_f+\Delta t) - \boldsymbol{R}_{\rm PLF}(t_f-\Delta t)\big)/2\Delta t$, and the similar formula folds for the TLF. In this way, we remove the kinetic energy of center-of-mass translational motion of the produced fragments before the particle number projection procedure performed.

***Step* (*ii*):** Up to now, we have developed formulas for a system composed of identical fermions. Let us consider the case of actual nuclei composed of two kinds of fermions (neutrons and protons). To calculate internal energy of the stopped fragment by the *Step* (*i*), we apply formulas of Eqs. (10-12). By taking the arbitrary operator as a total Hamiltonian of the system, $\hat{\mathcal{O}} = \hat{H} = \sum_i \hat{t}_i + \sum_{i<j}\hat{v}_{ij}$, we may evaluate internal energy of each particle number projected state. We note that, in the case of actual nuclei, we have to achieve the projection calculation for both neutrons and protons. We denote the particle number projection operator onto a n-particle state for neutrons as $\hat{P}^{(n)}_n$ and that for protons as $\hat{P}^{(p)}_n$. We use notation of the phase factor in the projection operator, θ for neutrons and φ for protons. If we use the Skyrme-like contact type interaction, we may obtain the following expression for internal energy of the

stopped fragments:

$$
\begin{aligned}
E_{n,z} &= \frac{\langle\Psi|\,\hat{H}\hat{P}_n^{(n)}\hat{P}_z^{(p)}\,|\Psi\rangle}{\langle\Psi|\,\hat{P}_n^{(n)}\hat{P}_z^{(z)}\,|\Psi\rangle} \\
&= \frac{1}{(2\pi)^2 P_n P_z}\int_0^{2\pi} d\theta \int_0^{2\pi} d\varphi\; e^{i(n\theta+z\varphi)}\det\mathcal{B}(\theta,\varphi) \\
&\qquad\qquad \times\big\langle\Psi\big|\hat{H}\big|\tilde{\Psi}(\theta,\varphi)\big\rangle \\
&= \frac{1}{(2\pi)^2 P_n P_z}\int_0^{2\pi} d\theta \int_0^{2\pi} d\varphi\; e^{i(n\theta+z\varphi)}\det\mathcal{B}(\theta,\varphi) \\
&\qquad \times\left(\int_{V_{\rm P}} d\boldsymbol{r}\;\tilde{\mathcal{H}}(\boldsymbol{r},\theta,\varphi) + \int_{V_{\rm T}} d\boldsymbol{r}\;\tilde{\mathcal{H}}(\boldsymbol{r},\theta,\varphi)\right) \\
&\equiv E_{n,z}^{\rm PLF} + E_{N-n,Z-z}^{\rm TLF}, \qquad (13)
\end{aligned}
$$

where $E_{n,z}^{\rm PLF}$ represents an internal energy of a produced fragment in the spacial region $V_{\rm P}$ containing n neutrons and z protons. Here, N and Z denote the total number of neutrons and protons in the whole system, respectively. In practice, we perform the two integrals over phase factor θ and φ employing the trapezoidal rule discretizing the interval $[0, 2\pi]$ into M equal grids. Because the Hamiltonian density, $\mathcal{H}(\boldsymbol{r})$, contains mixtures of proton and neutron densities, e.g. $\rho(\boldsymbol{r}) = \rho^{(n)}(\boldsymbol{r}) + \rho^{(p)}(\boldsymbol{r})$, we need to calculate both integrals simultaneously or, in other words, we need to calculate the Hamiltonian density $\tilde{\mathcal{H}}(\boldsymbol{r},\theta,\varphi)$, M^2 times. The center-of-mass correction for kinetic energy of each fragment is simply taken into account by replacing a coefficient of kinetic energy operator, $\hat{T} = \sum_i \hat{\boldsymbol{p}}_i/2m$, from $1/2m$ to $(1-1/a)/2m$ where $a = n + z$ denotes the mass number of the fragment. When we calculate the internal energy of the PLF (TLF), Coulomb energy of the other fragment is subtracted.

***Step (iii)*:** We then evaluate the excitation energy of the PLF fragment in the spacial region $V_{\rm P}$ containing n neutrons and z protons as

$$
E_{n,z}^{*} = E_{n,z}^{\rm PLF} - E_{n,z}^{\rm g.s.}, \qquad (14)
$$

where $E_{n,z}^{\rm g.s}$ is ground state energy with n neutrons and z protons. For the ground state energy $E_{\rm g.s}$, we use experimental values reported by G. Audi *et al.* [8] when available. When there is no available experimental data, we use the ground state energy reported by M.V. Stoitsov *et al.* employing Hartree-Fock-Bogoliubov theory with the Skyrme SLy4 effective interaction calculated by using two-center harmonic oscillator basis functions [9]. We note that, in the present work, the energy associated with collective rotational motion of the produced fragment is not removed from the energy, $E_{n,z}^{*}$, which should be distinguished from the internal excitation energy of the fragment.

E. Numerical methods

We have developed our own computational code of the TDHF theory for heavy-ion collisions extending the code developed for the real-time linear response calculations [10]. We employ a uniform spatial grid in the three-dimensional Cartesian coordinate to represent single-particle orbitals without any symmetry restrictions. The grid spacing is taken to be 0.8 fm. We take a box size of $50 \times 40 \times 20$ grid points (40 fm $\times$ 32 fm $\times$ 16 fm) for collision calculations, where the reaction plane is taken to be the xy-plane. The initial wave functions of projectile and target nuclei are prepared in a box with $20 \times 20 \times 20$ grid points. We use 11-points finite-difference formula for the first and second derivatives. To calculate the time evolution of single-particle orbitals, we use the Taylor expansion method of 4th order. The first-order predictor-corrector step is adopted in the time evolution. The time step is set to $\Delta t = 0.1$ fm/c. To calculate the Coulomb potential, we employ the Hockney's method [11] in which the Fourier transformation is achieved in the grid of two times larger box than that utilized to express single-particle orbitals.

III. RESULTS

In this section, we will show calculated results of ^{24}O+^{16}O reaction at incident energies of 800, 1600, 3200, 4800 MeV.

As for the energy density functional and potential, we use the Skyrme functional including all time-odd terms [12] except for the second derivative of the spin densities, $\triangle \boldsymbol{s}^{(n,p)}$. All of the results reported here are calculated using the Skyrme SLy5 parameter set [13]. This interaction has been utilized in the fully three-dimensional TDHF calculations for heavy-ion collisions [14–16]. In the ground state calculations, we find the ground states of ^{16}O and ^{24}O are spherical.

We take the incident direction parallel to the x-axis and the impact parameter vector parallel to the y-axis. The reaction is specified by the incident energy and the impact parameter. As an initial condition, the two colliding nuclei are placed with the distance 16 fm in the x-direction. Before starting the TDHF calculation, we assume the centers of the two colliding nuclei follow the Rutherford trajectory. We stop time evolution calculations when two nuclei are separated by 16 fm.

To investigate grazing reactions, we choose the impact parameter at which the same value of distance of closest approach, d, is achieved at each incident energy. Such an impact parameter is given by $b = \sqrt{d\,(d - (Z_{\rm P}Z_{\rm T}e^2)/E_{\rm rel})}$ where $E_{\rm rel}$ is incident relative energy. Reactions with the distance of closest approach of $d = R_0(A_{\rm P}^{1/3} + A_{\rm T}^{1/3})$ for $R_0 = 1.0$, 1.2, 1.5, 1.8 are calculated. As an example, in Fig. 1, we show time dependence of the relative distance between two center-of-masses of the colliding nuclei, $R_{\rm rel}(t)$, in ^{24}O+^{16}O reaction at several incident energies which give the same distance of closest approach $d = 1.5(A_{\rm P}^{1/3} + A_{\rm T}^{1/3})$. Red solid, green dashed, blue dotted, and purple broken lines represent a result at 800, 1600, 3200, and 4800 MeV,

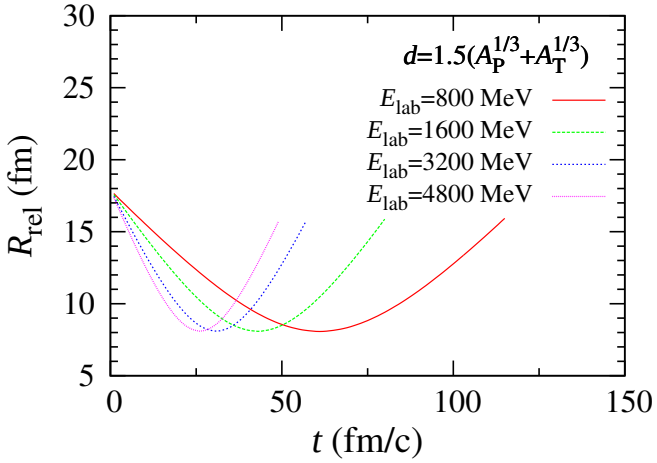

FIG. 1. Time dependence of the relative distance $R_{\rm rel}(t)$ in ^{24}O+^{16}O reaction at several incident energies which give the same distance of closest approach $d = 1.5(A_{\rm P}^{1/3} + A_{\rm P}^{1/3})$. Red solid, green dashed, blue dotted, and purple broken lines represent a result at 800, 1600, 3200, and 4800 MeV, respectively.

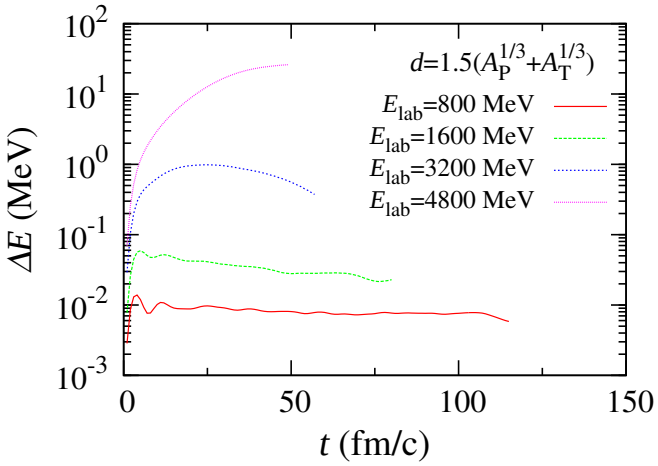

FIG. 3. Energy variance from total energy at the initial stage of the calculation during a time evolution in ^{24}O+^{16}O reaction at several incident energies which give the same distance of closest approach $d = 1.5(A_{\rm P}^{1/3} + A_{\rm P}^{1/3})$. Red solid, green dashed, blue dotted, and purple broken lines represent a result at 800, 1600, 3200, and 4800 MeV, respectively.

respectively. From the figure, we can see that the minima of curves $R_{\rm rel}(t)$ which corresponds to the distance of closest approach have almost the same value.

Before showing calculated results of physical quantities, let us show numerical accuracy in calculating grazing reactions at intermediate energy by the TDHF theory. Since, in the TDHF calculation, total number of nucleons in the whole system and total energy of the system are conserved during the time evolution, to check how the conservation properties are kept during the time evolution may provide information about the numerical accuracy.

Figure 2 shows difference in particle number from initial total number of nucleons, 40, during a time evolution in ^{24}O+^{16}O reaction at several incident energies which give the same distance of closest approach $d = 1.5(A_{\rm P}^{1/3} + A_{\rm P}^{1/3})$. Red solid, green dashed, blue dotted, and purple broken lines represent a result at 800, 1600, 3200, and 4800 MeV, respectively. Figure 2 shows that the total number of nucleons is nicely conserved during the time evolution. From the figure, we find that the conservation property of total number of nucleons

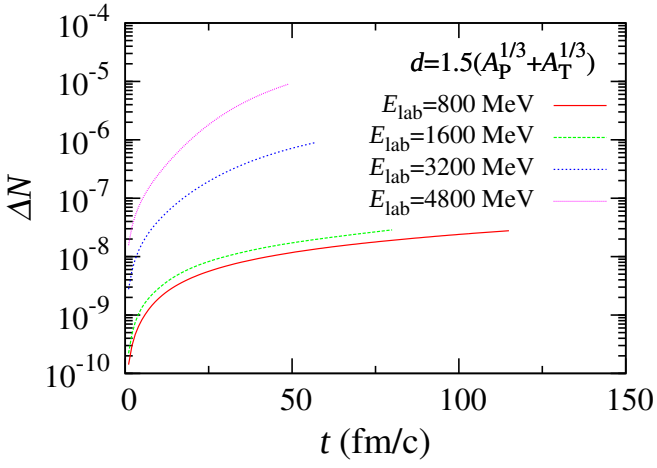

FIG. 2. Difference in particle number from initial total number of nucleons, 40, during a time evolution in ^{24}O+^{16}O reaction at several incident energies which give the same distance of closest approach $d = 1.5(A_{\rm P}^{1/3} + A_{\rm P}^{1/3})$. Red solid, green dashed, blue dotted, and purple broken lines represent a result at 800, 1600, 3200, and 4800 MeV, respectively.

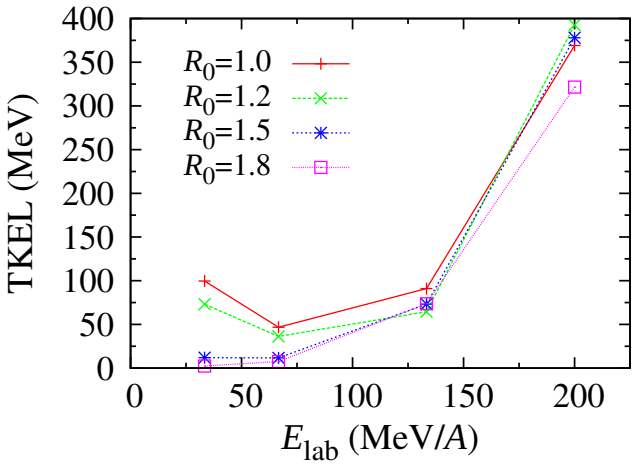

FIG. 4. Total kinetic energy loss (TKEL) as a function of incident energy $E_{\rm lab}$. Red pluses connected with solid lines, green crosses connected with dashed lines, blue stars connected with dotted lines, and purple open boxes connected with broken lines represent a result of a fixed value of distance of closest approach $d = R_0(A_{\rm P}^{1/3} + A_{\rm T}^{1/3})$ with R_0 = 1.0, 1.2, 1.5, and 1.8, respectively.

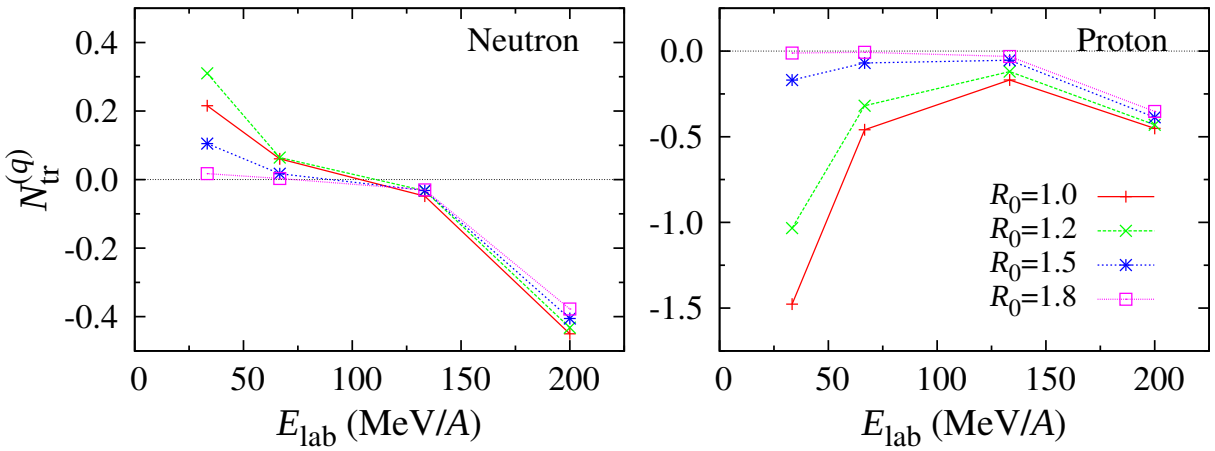

FIG. 5. Average number of transferred neutrons (left) and protons (right) from the projectile to the target as functions of incident energy $E_{\rm lab}$. Plus (minus) sign represents an increase (decrease) of number of nucleons in the target nucleus. Red pluses connected with solid lines, green crosses connected with dashed lines, blue stars connected with dotted lines, and purple open boxes connected with broken lines represent a result of a fixed value of distance of closest approach $d = R_0(A_{\rm P}^{1/3} + A_{\rm T}^{1/3})$ with $R_0 = 1.0$, 1.2, 1.5, and 1.8, respectively.

becomes less accurate as the incident energy increases. The difference in total number of nucleons ΔN reaches a value of 10^{-5} in the case of highest incident energy of $E_{\rm lab} = 4800$ MeV (200 MeV/A).

In Fig. 3, we show energy variance from total energy at the initial stage of the calculation during a time evolution in ^{24}O+^{16}O reaction at several incident energies which give the same distance of closest approach $d = 1.5(A_{\rm P}^{1/3} + A_{\rm P}^{1/3})$. Again, red solid, green dashed, blue dotted, and purple broken lines represent a result at 800, 1600, 3200, and 4800 MeV, respectively. As in the case of the total number of nucleons shown in Fig. 2, the conservation property becomes less accurate as the incident energy increases. In particular, the energy variance ΔE reaches a value of around 20 MeV in the case of $E_{\rm lab} = 4800$ MeV (200 MeV/A). I checked whether this conservation property is improved by changing the time step Δt to 0.01 fm/c. However, it turned out that the value ΔE was almost independent from the value of Δt. This fact may indicate that the time evolution is no longer solved precisely in the case of $E_{\rm lab} = 4800$ MeV. It may, to some extent, be improved if we use more smaller mesh spacing than $\Delta H = 0.8$ fm, however, I still not checked it and leaves it as a future task.

Next, in Fig. 4, we show total kinetic energy loss (TKEL) as a function of the incident energy $E_{\rm lab}$. Red pluses connected with solid lines, green crosses connected with dashed lines, blue stars connected with dotted lines, and purple open boxes connected with broken lines represent a result of a fixed value of distance of closest approach $d = R_0(A_{\rm P}^{1/3} + A_{\rm T}^{1/3})$ with $R_0 = 1.0$, 1.2, 1.5, and 1.8, respectively. From the figure, we find the TKEL takes substantially large value, more than 300 MeV when the incident energy becomes $E_{\rm lab} = 4800$ MeV (200 MeV/A). It would be considered as unphysical, since the distance of closest approach d with $R_0 = 1.8$ is around 9.7 fm which is larger than the sum of radius of the projectile and the target which should not result in such a high momentum transfer. We should keep in mind this unphysical deceleration when we calculate reactions at intermediate energy by the TDHF theory. I should also check whether this unphysical deceleration is removed if we take more small mesh spacing.

We next consider the average number of transferred nucleons. We denote the average number of nucleons in the TLF as $N_{\rm TLF}^{(q)}$ ($q = n$ for neutrons, p for protons), which is calculated from the density distribution at the final stage of the calculation,

$$N_{\rm TLF}^{(q)} = \int_{\text{around TLF}} d\boldsymbol{r}\ \rho^{(q)}(\boldsymbol{r}), \tag{15}$$

where $\rho^{(q)}(\boldsymbol{r})$ is the density distribution of neutrons ($q = n$) or protons ($q = p$). The spatial integration is achieved over a sphere whose center coincides with the center-of-mass of the TLF. The radius of the sphere is taken to be 8 fm. The average number of transferred nucleons from the projectile to the target, $N_{\rm tr}^{(q)}$, is given by

$$N_{\rm tr}^{(q)} = N_{\rm TLF}^{(q)} - N_{\rm T}^{(q)}, \tag{16}$$

where $N_{\rm T}^{(q)}$ denotes the initial number of neutrons ($q = n$) or protons ($q = p$) in the target nucleus.

Figure 5 shows the average number of transferred neutrons (left) and protons (right) from the projectile to the target as a function of incident energy $E_{\rm lab}$ for several values of the distance of closest approach, d. Red pluses connected with solid lines, green crosses connected with dashed lines, blue stars connected with dotted lines, and purple open boxes connected with broken lines represent a result of a fixed value of distance of closest approach $d = R_0(A_{\rm P}^{1/3} + A_{\rm T}^{1/3})$ with $R_0 = 1.0$, 1.2, 1.5, and 1.8,

respectively. In the case of the lowest energy $E_{\rm lab} = 800$ MeV ($\sim$33 MeV/A), we find neutrons are transferred from ^{24}O to ^{16}O and protons are transferred from ^{16}O to ^{24}O, the direction of charge equilibrium of the system. As the incident energy increases, the average number of transferred nucleons decreases. In the case of incident energy of $E_{\rm lab} = 3200$ MeV ($\sim$133 MeV/A), the number of transferred nucleons are very small, on average. In the case of $E_{\rm lab} = 4800$ MeV (200 MeV/A), both average number of transferred neutrons and protons become negative. Since this value is almost independent from the distance of closest approach, these nucleons might be unphysically emitted to the continuum during the time evolution.

Next, in Fig. 6, we show neutron (left column) and proton (right column) transfer probabilities from the projectile to the target for (-2), $\cdots$, $(+2)$ transfer channels as functions of incident energy $E_{\rm lab}$. The plus (minus) sign indicates an increase (decrease) of nucleons in the target nucleus. Red pluses connected with solid lines, green crosses connected with dashed lines, blue stars connected with dotted lines, and purple open boxes connected with broken lines represent a result of a fixed value of distance of closest approach $d = R_0(A_{\rm P}^{1/3} + A_{\rm T}^{1/3})$ with $R_0 = 1.0$, 1.2, 1.5, and 1.8, respectively. We can see relatively large values of probabilities in $(+2n)$, $(+1n)$, $(-1p)$, and $(-2p)$ panels (except for $(0n)$ and $(0p)$ panels). These directions of nucleon transfer are consistent with the observation in the average number of nucleons shown in Fig. 5. In the figure, we can see the probability for one neutron removal shown in $(-1n)$ panel which could not seen in the average number of nucleons shown in Fig. 5. In the case of $E_{\rm lab} = 4800$ MeV, probabilities for one neutron removal and one proton removal shown in $(-1n)$ and $(-1p)$ panels becomes sizable. This comes from unphysical emission of nucleons as shown in Fig. 5.

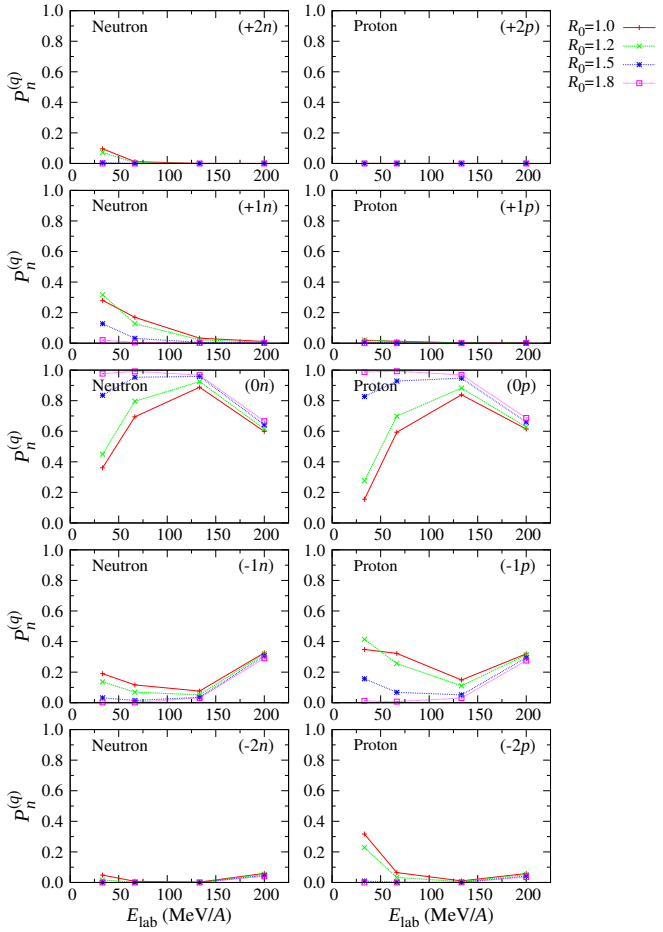

FIG. 6. Neutron (left column) and proton (right column) transfer probabilities as functions of incident energy $E_{\rm lab}$. The number of transferred nucleons are indicated as $(\pm xq)$ ($-2 \le x \le +2$, $q = n$ for neutrons and $q = p$ for protons). Red pluses connected with solid lines, green crosses connected with dashed lines, blue stars connected with dotted lines, and purple open boxes connected with broken lines represent a result of a fixed value of distance of closest approach $d = R_0(A_{\rm P}^{1/3} + A_{\rm T}^{1/3})$ with $R_0 = 1.0$, 1.2, 1.5, and 1.8, respectively.

Figure 7 shows excitation energy of the TLF in specific transfer channels as a function of the incident energy $E_{\rm lab}$. The excitation energy of the TLF is evaluated

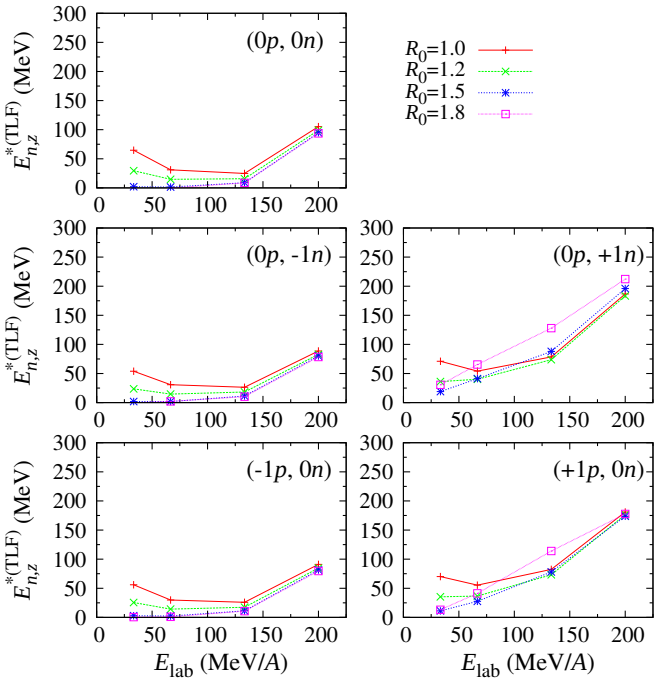

FIG. 7. Excitation energy of the TLF in specific transfer channels as a function of incident energy $E_{\rm lab}$. The number of transferred nucleons from the target ^{16}O is indicated as $(\Delta Z, \Delta N)$, where the plus (minus) sign corresponds to an increase (decrease) of number of nucleons in the target. Red pluses connected with solid lines, green crosses connected with dashed lines, blue stars connected with dotted lines, and purple open boxes connected with broken lines represent a result of a fixed value of distance of closest approach $d = R_0(A_{\rm P}^{1/3} + A_{\rm T}^{1/3})$ with $R_0 = 1.0$, 1.2, 1.5, and 1.8, respectively.

by using the projection procedure described in Sec. II D. The number of transferred nucleons from the target ^{16}O is indicated as $(\Delta Z, \Delta N)$, where the plus (minus) sign corresponds to an increase (decrease) of number of nucleons in the target nucleus. Red pluses connected with solid lines, green crosses connected with dashed lines, blue stars connected with dotted lines, and purple open boxes connected with broken lines represent a result of a fixed value of distance of closest approach $d = R_0(A_{\rm P}^{1/3} + A_{\rm T}^{1/3})$ with $R_0 = 1.0$, 1.2, 1.5, and 1.8, respectively. Looking at $(0p, 0n)$, $(0p, -1n)$, and $(-1p, 0n)$ panels (left column), we find that produced fragments have low excitation energy, especially for $R_0 = 1.5$ and 1.8 cases. On the other hand, in the cases of $(0p, +1n)$ and $(+1p, 0n)$ (right column), produced fragments are highly excited even if the R_0 value is 1.5 or 1.8. As the incident energy increases, the excitation energy of produced fragments also increases in the cases of $(0p, +1n)$ and $(+1p, 0n)$.

In this way, we can extract physical quantities from particle number projected states by applying the method described in Sec. II C and D.

IV. SUMMARY AND FUTURE PROSPECT

In this project work, we investigated that how the time-dependent Hartree-Fock (TDHF) theory works for grazing reaction at intermediate energy. We calculated grazing reaction in ^{24}O+^{16}O system at incident energies of 800, 1600, 3200, and 4800 MeV. For each incident energy, we calculated reactions with fixed values of the distance of closest approach $d = R_0(A_{\rm P}^{1/3} + A_{\rm T}^{1/3})$ for the R_0 values of 1.0, 1.2, 1.5, and 1.8. Using the particle number projection method which was recently proposed by C. Simenel we calculated transfer probabilities form the TDHF wave function after the collision. By applying the projection method, we also calculated excitation energy of produced fragment in specific transfer channels.

As increasing the incident energy, there appear some unphysical behaviors in calculated quantities, energy conservation property, total kinetic energy loss (TKEL), and average number of transferred nucleons. In the case of incident energy of 200 MeV/A, the energy variance from initial total energy of the system becomes around 20 MeV, and the TKEL becomes more than 200 MeV. The average number of transferred nucleons from the projectile to the target, in this case, has a negative value for both neutrons and protons indicating that some nucleons were unphysically emitted to the continuum during the time evolution. These unphysical behavior indicate that the time evolution in the TDHF theory is no longer solved accurately. We should calculate the same situation utilizing more small mesh spacing than that used value of 0.8 fm.

Looking at the results of TDHF calculation, the reaction dynamics was calculated without numerical instability up to around 100 MeV/A. What we should do next is to clarify how qualitatively/quantitatively the TDHF theory describes such a reaction at incident energy of around 100 MeV/A. Since the TDHF theory dose not contain effects of nucleon-nucleon collisions which expected to be important in reactions at such a relatively high incident energy, the TDHF theory is expected to fail to reproduce measured trends. However, because I think that to realize the limit of application is important for improving the method and for extending the application, I will continue this work until we uncover the applicability of the TDHF theory to reactions at relatively high incident energy of around 100 MeV/A.

ACKNOWLEDGMENTS

I would like to thank the organizers and the lectures for their enthusiasm, activities, and kindness. I am very much grateful to all of the organizers, lecturers, and other staffs of GANIL for preparing and organizing a wonderful period of the TALENT school. Indebted for their helps, supports, and efforts, I have obtained special experience during the school without any problem. I would certainly hope to take part in further courses, as possible.

[1] P.A.M. Dirac, Proc. Cambridge Philos. Soc. **26**, 376 (1930).
[2] P. Bonche, S. Koonin, and J.W. Negele, Phys. Rev. C **13**, 1226 (1976).
[3] C. Simenel, Eur. Phys. J. A **48**, 152 (2012).
[4] K. Sekizawa and K. Yabana, Phys. Rev. C **88**, 014614 (2013).
[5] C. Simenel, Phys. Rev. Lett. **105**, 192701 (2010).
[6] S. Shinohara, H. Ohta, T. Nakatsukasa, and K. Yabana, Phys. Rev. C **88**, 054315 (2006).
[7] K. Sekizawa and K. Yabana, In preparation.
[8] G. Audi, A.H. Waspstra, and C. Thibault, Nucl. Phys. **A729**, 337 (2003).
[9] M.V. Stoitsov, J. Dobaczewski, W. Nazarewicz, S. Pittel, and D.J. Dean, Phys. Rev. C **68**, 054312 (2003).
[10] T. Nakatsukasa and K. Yabana, Phys. Rev. C **71**, 024301 (2005).
[11] J.W. Eastwood and D.R.K. Brownrigg, J. Compt. Phys. **32**, 24 (1979).
[12] J. Dobaczewski and J. Dudek, Phys. Rev. C **52**, 1827 (1995).
[13] E. Chabanat, P. Bonche, P. Haensel, J. Meyer and R. Schaeffer, Nucl. Phys. **A635**, 231 (1998); **A643**, 441 (1998).
[14] A.S. Umar and V.E. Oberacker, Phys. Rev. C **73**, 054607 (2006).
[15] A.S. Umar and V.E. Oberacker, Phys. Rev. C **77**, 064605 (2008).
[16] R. Keser, A.S. Umar, and V.E. Oberacker, Phys, Rev. C **85**, 044606 (2012).